Identification of RNA-targeting Small Molecule Inhibitors for Enterovirus A71 IRES by Structure-Based Virtual Screening

Kaichen Wang, [a‡] *Sean Xian Yu Lee,* [a‡] *Chaitanya K. Jaladanki,* [b] *Wei Shen Ho,* [a] *Justin Jang Hann Chu,* [c] *Hao Fan,* [b,d,e*] *Christina Li Lin Chai* [a*]

AUTHOR ADDRESS

a. Department of Pharmacy and Pharmaceutical Sciences, Faculty of Science, National University of Singapore, Block S4A, Level 3, 18 Science Drive 4, 117543, Singapore

b. Bioinformatics Institute, Agency for Science, Technology and Research (A*STAR), 30 Biopolis Street, Matrix #07-01, Singapore 138671, Singapore

c. Laboratory of Molecular RNA Virology and Antiviral Strategies, Department of Microbiology and Immunology, Yong Loo Lin School of Medicine, National University of Singapore, 5 Science Drive 2, 117545, Singapore

d. Synthetic Biology Translational Research Program and Department of Biochemistry, Yong Loo Lin School of Medicine, National University of Singapore, 10 Medical Drive, Singapore 117597.

e. Duke-NUS Medical School, 8 College Rd, Singapore 169857, Republic of Singapore

[‡]These authors contribute equally

[*]Corresponding authors. Email: fanh@bii.a-star.edu.sg (H.F.) and phacllc@nus.edu.sg (C.L.L.C.)

ABSTRACT

Structured RNAs play a crucial role in regulating gene expression, which includes both protein synthesis and RNA processing. Dysregulation of these processes is associated with various conditions, including viral and bacterial infections, as well as cancer. The unique tertiary structures of structured RNAs provide an opportunity for small molecules to directly modulate such processes, making them promising targets for drug discovery. Although small-molecule inhibitors targeting RNA have shown early success, *in silico* strategies like structure-based virtual screening remain underutilized for RNA-targeted drug discovery. In this study, we developed a virtual screening scheme targeting the structural ensemble of EV-A71 IRES SL II, a non-coding viral RNA element essential for viral replication. We subsequently optimized the experimentally validated hit compound IRE-03 from virtual screening through “analog-by-catalog” search. This led to the identification of a more potent IRES inhibitor, IRE-03-3, with an EC_{50} value of 11.96 μM against viral proliferation. Our findings demonstrate that structure-based virtual screening can be effectively applied to RNA targets, providing exciting new opportunities into future antiviral drug discovery.

KEYWORDS: Virtual Screening, Drug Discovery, Structured RNA, Antiviral, EV-A71 IRES

INTRODUCTION

Over the past few decades, molecular biology has revealed the widespread presence of structured RNAs in bacteria, viruses, and eukaryotic organisms. These structured RNAs play crucial roles in biological processes, particularly in the regulation of gene expression, RNA splicing and protein synthesis. For example, riboswitches, which are commonly found in the non-coding region of bacterial mRNA, regulate gene expression by direct binding of small molecule ligands.[1-3] The transactivation response (TAR) element of human immunodeficiency virus (HIV) is a small structured RNA crucial for viral replication, as it can interact with the Tat protein to enhance transcription of the viral genome.[4-8] In human cells, the long non-coding RNA (lncRNA) metastasis-associated lung adenocarcinoma transcript 1 (MALAT1) regulates alternative splicing and transcription. Its dysregulation is often associated with cancer development and progression.[9-11] The above evidence highlights the essential roles of structured RNAs in regulating physiological and pathological processes, making these structured RNAs promising targets for drug discovery and further emphasizing the potential of RNA-targeting therapeutics.

While RNA-targeting strategies such as antisense oligonucleotide (ASO)[12,13] and small interfering RNA (siRNA)[14,15] have gained much attention, small molecule drugs offer significant advantages in terms of drug delivery and safety compared to these nucleic acid-based therapies.[16-18] Although small molecule RNA-targeting therapeutics are less prominent relative to small molecules that target proteins, there have been significant progress on this front in the past few decades. For example, a large subset of first-line antibiotics such as aminoglycosides, tetracyclines and macrolides were found to exhibit their activity by binding at structured regions in bacterial ribosomal RNA, thereby inhibiting bacterial protein synthesis.[19] Additionally, small molecules

have been identified to target riboswitches such as the flavin mononucleotide (FMN) riboswitch,[20,21] pre-Q1 riboswitch[22] and tetrahydrofolate (THF) riboswitch[23,24] in bacterial genome with nanomolar level of potency, suggesting the potential of riboswitches as targets in future antibiotics drug development. Small molecules have also been shown to bind to structured regions of viral RNA, such as the internal ribosomal entry site (IRES) of hepatitis C virus (HCV)[25,26] and the frameshifting pseudoknot element (FSPE)[27] of SARS-CoV-2, thereby inhibiting viral proliferation. Recently, the small molecule drug Risdiplam has been approved by FDA for the treatment of spinal muscular atrophy (SMA), a genetic neuromuscular disorder caused by mutation or deletion in the survival motor neuron (SMN) gene.[28] Risdiplam binds at the splicing site of exon 7 of the *SMN2* gene, promoting the production of functional SMN2 proteins and thereby slowing the progression of SMA.[29,30] These findings highlight the potential of RNA-targeting small molecule drugs.

Despite the successful discoveries of RNA-targeting small molecules, it is noted that most hits arise from experimental high throughput screening or via screening derivatives of known ligands. The limited diversity of compounds within existing chemical libraries also restricts the discovery of novel inhibitor scaffolds. Furthermore, the process is often time-consuming and labor-intensive. In contrast, computational approaches, particularly structure-based virtual screening, offer the potential to accelerate the identification of RNA-targeting small molecules.[31,32] While these structure-based methods, such as molecular docking are well-established for protein targets, most of them are not optimized against RNA targets, resulting in their limited applications in RNA-focused drug discovery.[33-35] One key challenge for the application of structure-based virtual screening is the unique properties of RNA, particularly its intrinsic flexibility and negatively

charged backbone, which can lead to uncertain performance for current tools.[36,37] Therefore, these methods should be carefully validated when applied to target RNA.

Enterovirus-A71 (EV-A71) is one of the main pathogens of the highly contagious disease Hand, Foot, and Mouth Disease (HFMD) that mainly targets children under 3 years old. Among the pathogens of HFMD, infection by EV-A71 often leads to more severe outcomes, including neurological disorders and deaths.[38] To date, significant efforts have been made in the development of antivirals against EV-A71 through targeting viral proteins such as the main protease $3C^{pro}$,[39,40] capsid protein VP1[41-43] and the RNA polymerase $3D^{pol}$.[44] However, there remains no effective small molecule therapeutics against EV-A71. Besides the viral proteins of EV-A71, the IRES in the 5'-untranslated region (UTR) of the viral genome plays crucial roles in viral replication. The IRES is made up of five structured RNA elements named stem loop (SL) II-VI in the 5'-UTR. Like other viral IRESs, these structured RNA elements can interact with host proteins to promote viral genome expression,[45,46] among which the SL II can form a complex with the host protein hnRNP A1 and stimulate translation of viral genome.[47,48] Davila-Calderon et al. [49] have shown that the small molecule inhibitor DMA-135 binds to the SL II of IRES, promoting the formation of a complex between SL II and another host factor AUF1 instead of hnRNP A1, thereby inhibiting viral proliferation. Given the lack of FDA-approved therapies for HFMD, targeting the EV-A71 IRES offers a potential therapeutic strategy to address this significant public health concern of HFMD.

Here we investigate the utility of molecular docking as a site-directed approach to discover new ligands for the DMA-135 binding site in SL II. First, from the structural ensemble of IRES SL II

(PDB: 6XB7), we selected the optimal NMR conformer for docking. Next, we screened a chemical library of ~11,000,000 compounds from ZINC 20[50] with a pharmacophore model generated from the selected NMR conformer. We then docked the compounds yielded from pharmacophore screening against the selected SL II conformer with RxDock.[51] Based on their docking scores and predicted binding poses, 13 compounds were shortlisted by visual inspection (Figure S1). Among the virtual screening hits, IRE-03 reduced IRES-mediated translation by 40% and inhibited viral proliferation with EC_{50} of 46.79 μM. Finally, we docked commercially available analogs of IRE-03 against IRES SL II, from which IRE-03-3 was identified to inhibit IRES activity and viral proliferation with much better potency than IRE-03. At the highest non-toxic concentration, IRE-03-3 achieved 45% inhibition of IRES-mediated translation and inhibition of viral proliferation in cells with an EC_{50} value of 11.96 μM. In summary, we discovered 3,4-diayl pyrazole scaffolds to be promising for the development of EV-A71 IRES inhibitors and demonstrated the feasibility of virtual screening for RNA targets.

RESULTS

Evaluation of the EV-A71 IRES SL II NMR structural ensemble

As outlined in our virtual screening workflow (Figure 1), the initial step of virtual screening is the evaluation of receptor conformations. The only available holo structure of EV-A71 IRES SL II comprises an ensemble of ten NMR conformers (PDB ID: 6XB7). The superimposition of conformers (Figure S2) based on RNA backbone yielded root mean square deviation (RMSD) values exceeding 4 Å for the RNA backbone in 40 out of 45 alignments and for the heavy atoms of the native ligand DMA-135[49] in 39 out of 45 alignments between individual NMR conformers and their corresponding ligands (Table S1, S2). These findings indicate that the SL II can adopt more than one distinct conformation. For virtual screening, we evaluated all ten conformers of the NMR ensemble to identify the most suitable NMR conformer for ligand binding. First, we docked the native ligand DMA-135[49] against each conformer using RxDock and calculated the RMSD of the best-scored docking poses relative to their native binding poses. The docking pose of DMA-135 against 3rd, 6th, 7th, and 9th conformers exhibited better RMSD values of 2.12, 1.77, 1.83 and 2.19 Å compared to other conformers (Table 1). Second, we docked a set of five ligands from the study reported by Davila-Calderon et al.[49] (Table S3) and their respective DUD-E decoys[52] against all conformers with RxDock to evaluate which conformer(s) show better ligand enrichment. The logarithmic area under the curve (logAUC) values of each conformer indicated that all conformers have good ligand enrichment (logAUC of 55.5-58.7) except for the 3rd conformer, which exhibited a lower logAUC value of 53 compared to the other conformers (Table 1). Third, we performed Molecular Mechanics/Generalized Born-Surface Area (MM-GBSA) rescoring for the native ligands in all the ten NMR conformers. The predicted binding free energy (ΔG_{Bind}) values are listed in Table 1. Notably, the 3rd and 9th conformers exhibit better ΔG_{Bind} values of -38.81 and -37.99 kcal/mol, respectively for native binding modes, with the 9th conformer achieving the best ΔG_{Bind}

value of -32.18 kcal/mol for redocked poses. Based on the RMSD values, ligand enrichment and MM-GBSA rescoring, we chose the 9^{th} conformer for further virtual screening study.

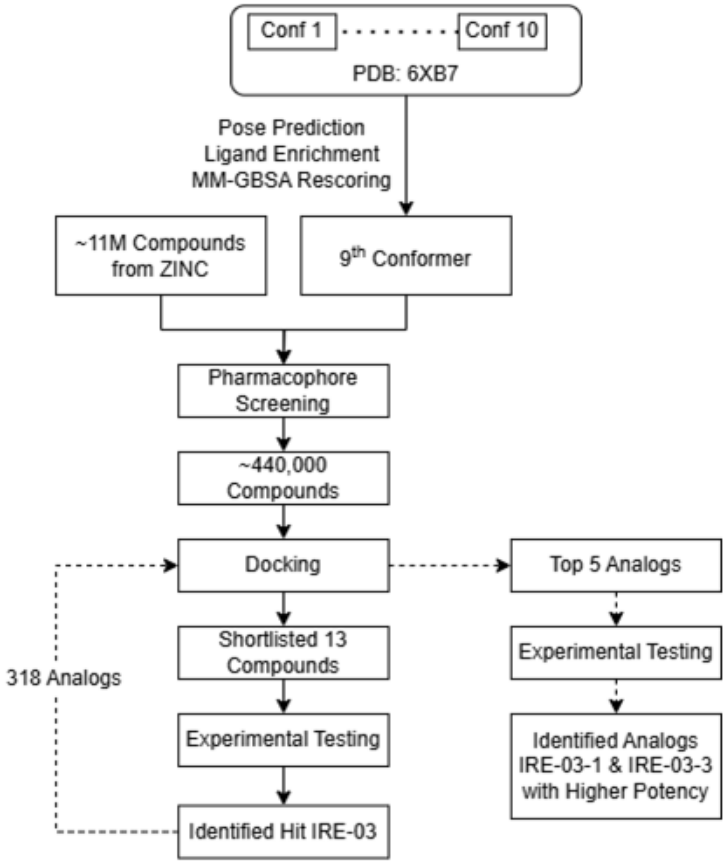


Figure 1. The workflow for virtual screening.

Table 1. The RMSD values of DMA-135, the logAUC values, and the binding free energy of the 10 NMR conformers/redock poses from MM-GBSA.

Conformer	RMSD (Å)	logAUC	Binding free energy for native poses (kcal/mol)	Binding free energy for redock poses (kcal/mol)
1st	6.00	57.2	-36.42	-13.90
2nd	8.30	56.2	-37.23	-28.93
3rd	2.12	53.0	-38.81	-21.18
4th	8.75	55.5	-31.46	-19.24
5th	8.60	58.7	-34.52	-4.84
6th	1.77	57.5	-30.43	-17.02
7th	1.83	57.5	-30.12	-18.49
8th	7.78	58.7	-27.95	-9.35
9th	2.19	57.2	-37.99	-32.18
10th	8.21	56.7	-34.66	-28.60

Pharmacophore Modeling

A pharmacophore model based on seven key features of the native ligand DMA-135 in 9th conformer (Figure S2) was generated to screen the ~11,000,000 “in-stock” compounds from ZINC 20. In the model, the 2-amino-6-dimethylamino pyrazine group was represented with one aromatic ring and hydrogen bond donor feature. Three hydrogen bond donors and one hydrogen bond acceptor features mimic the RNA-ligand interactions of guanidino moiety, and the phenyl group linked by the triple bond was also included as another aromatic ring. From screening, ~440,000 compounds that matched four out of seven features were retrieved for molecular docking.

Molecular docking based virtual screening and post-docking analysis

Approximately 440,000 compounds obtained from pharmacophore mapping were docked against the 9th conformer using RxDock. The top 2% compounds from docking were then filtered with the geometry filter derived from the 9th conformer. The compound must (1) make at least two hydrogen bonds with residues C5-G10/U35-A38 and (2) pi-pi stacking with residue G10. This filtering process yielded 2,204 compounds, which were clustered based on molecular similarity with a Tanimoto coefficient (Tc) cutoff of 0.75, using daylight-type linear fingerprints. Compounds from two of the 14 most populated clusters were excluded, as their scaffolds were identified as PAINS (pan-assay interference compounds), which are known to potentially lead to false positives in bioassays. From the remaining 12 clusters, two rounds of visual inspection were conducted based on the docking poses. Initially, 4-8 compounds were selected from each cluster, from which 13 compounds were then shortlisted as potential hits (Table S2).

Experimental validation of virtual screening hits

To determine the inhibition of IRES-mediated translation, the virtual screening hits were assayed using a previously validated bicistronic luciferase reporter construct.[53] The construct consisted of a Renilla luciferase (RLuc) reporter gene regulated by a human cytomegalovirus (CMV) promoter sequence and a Firefly luciferase (FLuc) reporter gene regulated by EV-A71 IRES (Figure 2A). The bicistronic luciferase construct was designed to simultaneously monitor both IRES-mediated, cap-independent translation[54] and cap-dependent translation based on FLuc and RLuc levels, respectively. In doing so, selective IRES inhibitors can be identified from non-selective translational inhibitors. The levels of both reporter enzymes were quantified based on the surrogate measure of bioluminescence intensity upon addition of the appropriate substrates.

The cytotoxicity profile of the virtual screening hits was first determined using alamarBlue™ cell viability reagent (Figure S5). Then, the compounds were screened for inhibition of IRES-mediated translation at the determined non-cytotoxic concentrations. Amongst the tested compounds, four compounds (IRE-03, IRE-07, IRE-12 and IRE-13) were found to inhibit IRES-mediated translation by at least 20% (Figure 2A).

In view that some heterocyclic compounds could be potential inhibitors of firefly luciferase,[55] an orthogonal FLuc enzymatic inhibition assay was designed and carried out to confirm that the decrease in the observed bioluminescence intensity was due to the decrease in IRES-mediated translation as opposed to inhibition of FLuc catalytic activity. Based on our results, IRE-03 demonstrated the least FLuc inhibition and was thus chosen for further studies (Figure S6). Subsequent viral plaque reduction assay results found that IRE-03 was able to reduce viral titer of EV-A71 by 1-$\log_{10}$ at its highest non-toxic concentration (Figures 2B-C). Notably, the EC_{50} value (EC_{50} = 46.79 μM) closely matches the observed initial decrease in IRES-mediated translation (Figure 2D). Additionally, the low maximum similarity value of 0.076 (Tc, Tanimoto coefficient) against reported IRES SL II binders[49] indicated that IRE-03 possesses a distinct scaffold from currently reported IRES inhibitors. Taken together, our results suggested that IRE-03 is a true inhibitor of IRES.

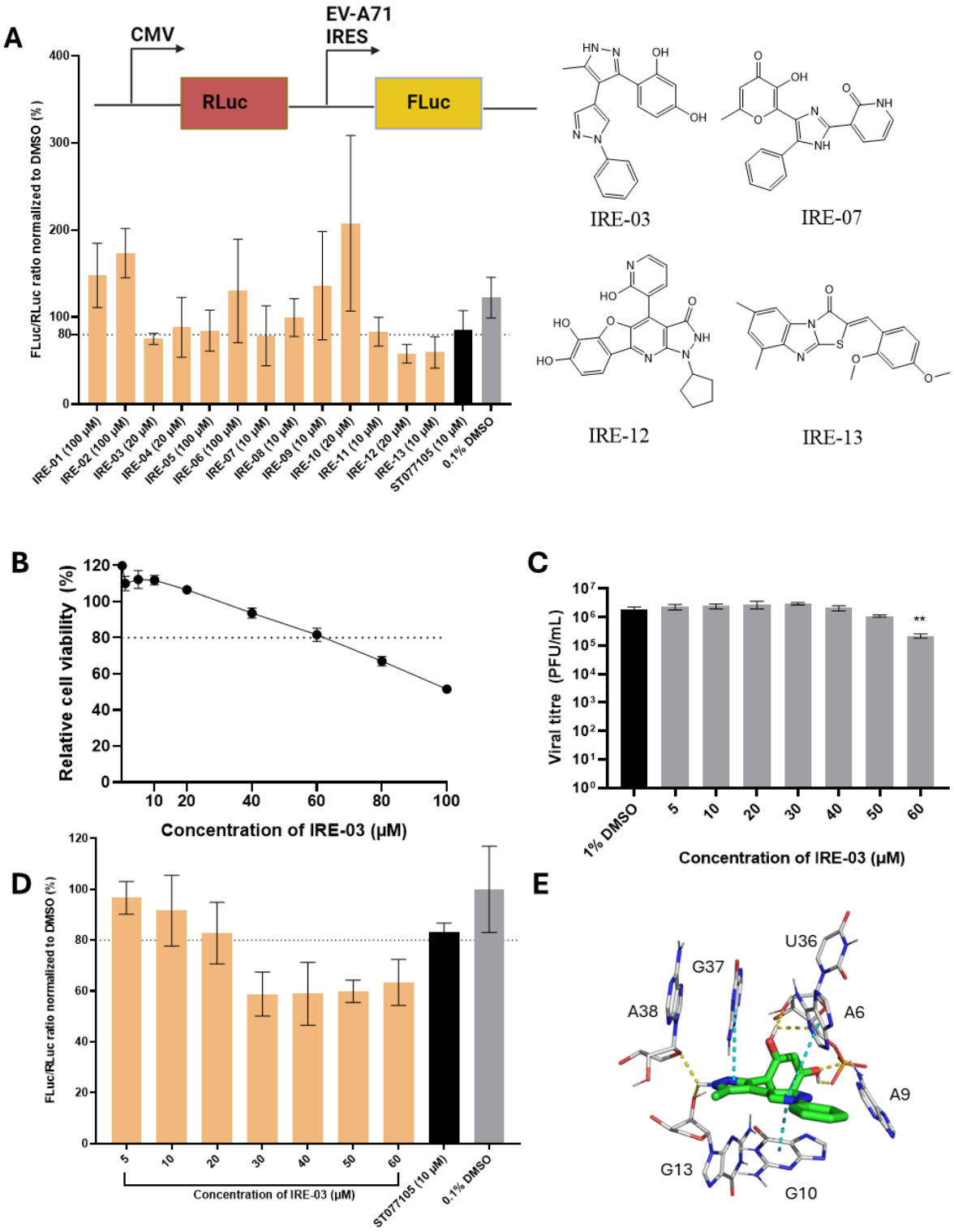


Figure 2. (A) Inhibition of EV-A71 IRES-mediated translation by the virtual screening hits at 20 or 100 μM. Dashed line indicates the 20% inhibition cut-off used in this study. Data is presented

as mean ± standard deviation. Structures of compounds found to inhibit IRES-mediated translation by at least 20% are shown. ST077105 was tested as the positive control for inhibition of EV-A71 IRES-mediated translation.[53] (B) Cytotoxicity profile of IRE-03, tested up to 100 μM. Dashed line indicates the 80% cell viability threshold used in this study. (C) Inhibition of EV-A71 viral proliferation in cells. Statistical significances were evaluated using one-way ANOVA and Dunnett's test. * denotes $p<0.05$, ** denotes $p<0.01$ and *** denotes $p<0.001$. (D) IRE-03 expressed dose-dependent inhibition of EV-A71 IRES-mediated translation. Dashed line indicates the 20% inhibition cut-off used in this study. ST077105 was tested as the positive control for inhibition of EV-A71 IRES-mediated translation.[53] (E) Structure and docking geometry of IRE-03. The ligand and receptor are colored green and grey, respectively. Hydrogen bonds and pi-pi stacking interactions between the ligand and receptor are depicted with yellow and cyan dashed lines, respectively. All cytotoxicity, viral proliferation and bicistronic luciferase reporter assays were performed using human RD cells (CCL-136, ATCC).

Analog search

The IRES inhibitory activity of the initial hit compound IRE-03 could be improved further through analog search. To identify analogs with higher potency, we collected 318 analogs from the ZINC catalog with substructure search by Tc similarity cutoff of 0.5 to IRE-03. Next, the analogs were docked to the 9th NMR conformer. To avoid compounds that could inhibit the activity of FLuc, the 110 analogs that scored equal or better than the native ligand, DMA-135, were filtered with the ChemFLuc webserver.[56] The webserver predicted FLuc inhibitor probability values above the cutoff of 0.3 for 7 out of the 110 analogs, which were removed from the list. The binding modes of the remaining 103 analogs were visually inspected, from which 5 analogs were shortlisted and

tested with the assays described in the previous section. Among the five analogs, three analogs (IRE-03-1, IRE-03-3 and IRE-03-4) were deemed to be promising IRES inhibitors at the highest non-toxic concentration (Figure 3A-B). However, IRE-03-4 was observed to also inhibit cap-dependent translation and FLuc catalytic activity (Figures S7, S8). Thus, only analogs IRE-03-1 and IRE-03-3 (with max Tc to known EV-A71 IRES SL II binders of 0.071 and 0.065 respectively) were further evaluated for their ability to inhibit IRES-mediated translation in a dose-dependent manner as well as to inhibit viral proliferation in cells (Figures 3C-E). To further validate the inhibitory effects of IRE-03-1 and IRE-03-3 on viral translation (over viral replication), we further constructed EV-A71 replication-competent and replication-defective RNA replicons based on a previously established protocol in our group.[57,58] In both replicons, genes encoding for viral structural proteins (VP1-4) were replaced with a Nanoluciferase reporter gene. The replication-competent replicon contains an intact $3D^{pol}$ region encoding the RNA-dependent RNA polymerase. Hence, it retains the ability to self-replicate and produce additional RNA copies that can be translated to nanoluciferase. Conversely, the replication-defective replicon contains a 159-nucleotide deletion which renders the RNA-dependent RNA polymerase non-functional. As a result, nanoluciferase expression is limited by translation of the original replicon. In brief, inhibition of viral translation would result in decreased nanoluciferase expression in both replicons while inhibition of viral replication would result in decreased nanoluciferase expression in only the replication-defective replicon. Guanidine hydrochloride (GuHCl)[59] and cycloheximide (CHX)[60] were used as positive controls for RNA replication and general translation, respectively. As IRE-03-1 and IRE-03-3 demonstrated a dose-dependent inhibition of luciferase expression in both replicons (Figure S9), this supports that IRE-03-1 and IRE-03-3 inhibits translation. Specifically, these compounds inhibited viral translation without affecting host translational

machinery as a decrease in cap-dependent translation was not observed in the bicistronic luciferase reporter assay.

Lastly, we functionally validated the inhibition of IRES-mediated translation by IRE-03-1 and IRE-03-3 resulted in antiviral activity. The better performing analog, IRE-03-3, demonstrated 45% inhibition of IRES-mediated translation at the highest non-toxic concentration and inhibition of viral proliferation in cells with a value of EC_{50} = 11.96 μM.

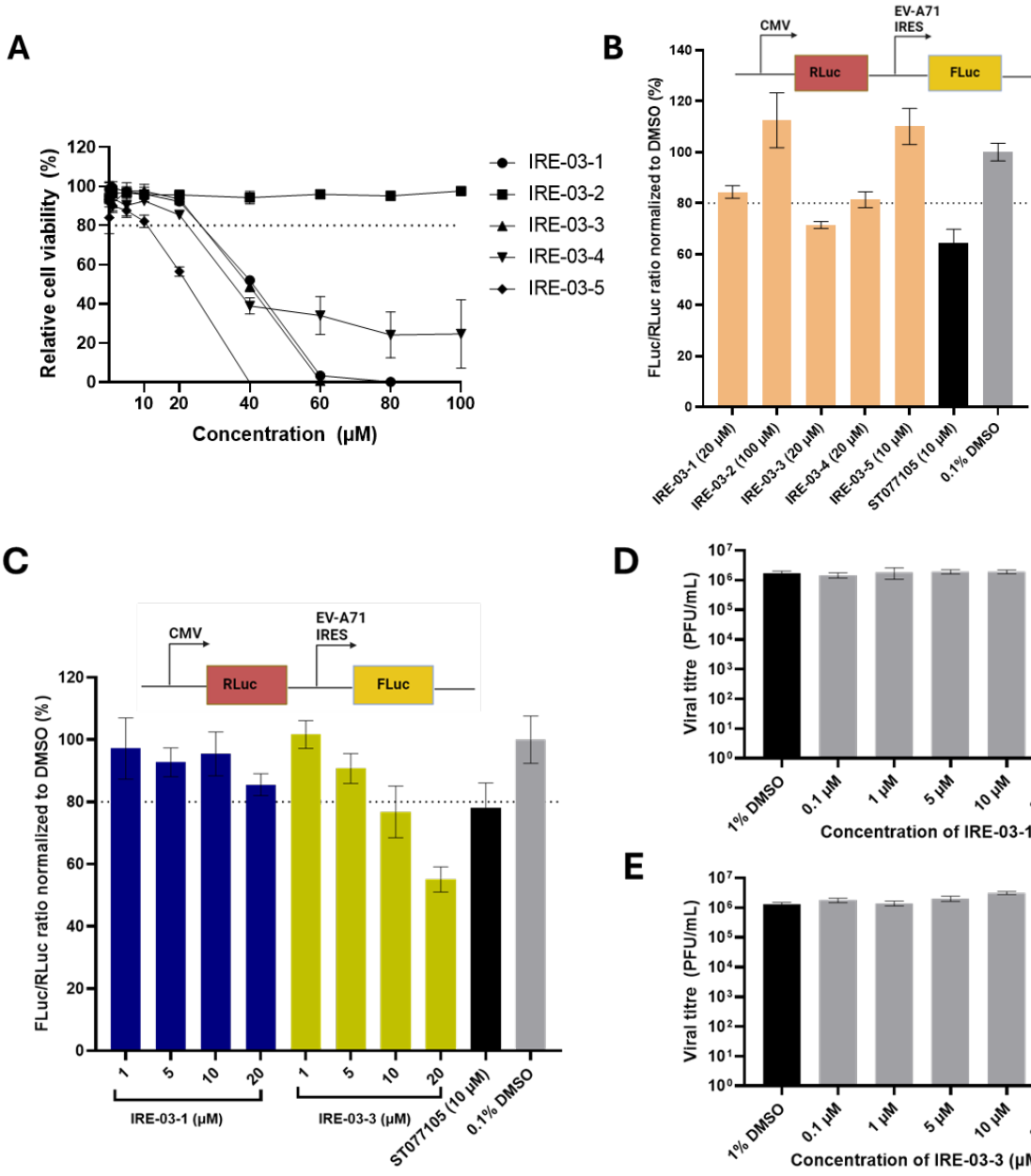

A
Relative cell viability (%)
Concentration (μM)
IRE-03-1
IRE-03-2
IRE-03-3
IRE-03-4
IRE-03-5
B
CMV
EV-A71 IRES
RLuc
FLuc
FLuc/RLuc ratio normalized to DMSO (%)
IRE-03-1 (20 μM)
IRE-03-2 (100 μM)
IRE-03-3 (20 μM)
IRE-03-4 (20 μM)
IRE-03-5 (10 μM)
ST077105 (10 μM)
0.1% DMSO
C
FLuc/RLuc ratio normalized to DMSO (%)
IRE-03-1 (μM)
IRE-03-3 (μM)
ST077105 (10 μM)
0.1% DMSO
D
Viral titre (PFU/mL)
1% DMSO
0.1 μM
1 μM
5 μM
10 μM
20 μM
Concentration of IRE-03-1 (μM)
E
Viral titre (PFU/mL)
Concentration of IRE-03-3 (μM)
F
U36
G37
A6
A38
G13
G10
IRE-03-1
IRE-03-3

Figure 3. Cytotoxicity profile, inhibitory activities and docking poses of all IRE-03 analogs on IRES-mediated translation. All data are presented as mean ± standard deviation. (A) The cytotoxicity profile of IRE-03 analogs. All analogs were tested up to 100 μM. Dashed line indicates the 80% cell viability threshold used in this study. (B) Inhibition of EV-A71 IRES-mediated translation of IRE-03 analogs. Dashed line indicates the 20% inhibition cut-off used in this study. ST077105 was tested as the positive control for inhibition of EV-A71 IRES-mediated translation.[53] (C) IRE-03-1 and IRE-03-3 exhibits dose-dependent reduction of IRES-mediated translation. (D, E) Inhibition of EV-A71 viral proliferation in cells by IRE-03-1 and IRE-03-3. Statistical significances were evaluated using one-way ANOVA and Dunnett's test. * denotes $p<0.05$, ** denotes $p<0.01$ and *** denotes $p<0.001$. (F) Structures and docking poses of analogs IRE-03-1 and IRE-03-3. The ligand and receptor are colored green and grey, respectively. All cytotoxicity, viral proliferation and bicistronic luciferase reporter assays were performed using human RD cells (CCL-136, ATCC).

DISCUSSION

Most available small molecule antiviral drugs target viral proteins but often encounter challenges such as drug resistance and off-target effects.[61] As an emerging strategy, small molecules targeting viral RNA expand the range of therapeutic targets and offer a potential solution to bypass drug resistance.[16-18,62] To target EV-A71 IRES, we selected the optimal NMR conformer from the structural ensemble (PDB: 6XB7) using molecular docking and MM-GBSA rescoring. Given the limited availability of ligands and PDB structures for our target, we generated a pharmacophore model to screen the ZINC 20 chemical library. Our virtual screening strategy, which integrated both pharmacophore screening and molecular docking, led to the identification of inhibitor IRE-03 and its analogs IRE-03-1 and IRE-03-3, all featuring a 3,4-diaryl pyrazole scaffold for inhibition. The *in vitro* activities of IRE-03 and its analogs were validated experimentally, and our results suggested the potential of virtual screening methods and offer insights that may guide future research on RNA-targeted drug discovery.

Studies have demonstrated that accounting for receptor flexibility could improve the accuracy of virtual screening.[63,64] However, selecting representative conformers from a structural ensemble remains challenging.[65] In this study, we applied the "selection by ligand" approach, prioritizing conformer(s) that demonstrated the best ligand binding. Given the multiple conformations that IRES SL II can adopt, this strategy helped to reduce computational costs. We supplemented molecular docking with the physics-based method MM-GBSA rescoring, which provided a more accurate prediction of binding free energies yet remained computationally efficient. From the results of molecular docking and MM-GBSA rescoring, the 9th conformer of IRES SL II was selected for its favorable RMSD (2.19 Å), ligand enrichment (57.2), and binding free energy (-47.68 kcal/mol). While our approach proved effective for virtual screening, future studies may also

benefit from exploring RNA target dynamics with more comprehensive sampling and evaluation techniques.

While the efficacy of pharmacophore mapping has been validated against protein targets, it remained underused for RNA targets. In previous studies, pharmacophore screening has been successfully applied against HCV IRES[66] and HIV TAR.[67] However, unlike these well-studied targets, EV-A71 IRES SL II has limited ligands and RNA-ligand complexes, making it difficult to conduct structure-activity relationship (SAR) analysis to identify key RNA-ligand interactions. Thus, in our study, a pharmacophore model based on all the RNA-ligand interactions in the 9th NMR conformer was generated. Along with molecular docking, the application of which led to the identification of the inhibitor IRE-03 and its analogs with enhanced potency from the virtual screening. Analysis of the docking poses of IRE-03 and its analogs, IRE-03-1 and IRE-03-3, suggested that their binding modes resemble that of the native ligand (Figures 2E, 3F). The bipyrazole core of IRE-03 and its analogs interact with residues G6/G10 and A38 through pi-pi stacking and hydrogen bonding, mirroring the interaction of the 2-amino-6-dimethylamino pyrazine group in DMA-135. However, the resorcinol/phenyl ether moiety in IRE-03 and its analogs adopted a slightly different orientation compared to the guanidino moiety of the native ligand, forming hydrogen bonds with residues G13/U35/U36. These pi-pi stacking and hydrogen bond interactions indicate that IRE-03 binds strongly to IRES SL II, stabilizing the complex.

While the experimental screening procedure identified IRE-03 and its analogs as IRES inhibitors, assay interference remains a potential confounding factor. The dual luciferase reporter assay used in our study is a bioluminescence-based method commonly applied to evaluate the

effects of small molecules on gene expression.[68] The design of our reporter plasmid (Figure 2A) allows for precise monitoring of changes in the IRES-mediated, cap-independent and cap-dependent gene expression through simultaneous measurement of bioluminescence intensity from FLuc and RLuc. Despite the sensitivity and versatility of the assay, it has been reported that molecules with different scaffolds can directly modulate the bioluminescence activity of FLuc, resulting in false positive results.[69,70] To address this, our study applied both orthogonal assay and *in silico* prediction to validate the affinity of the hit compounds for IRES. In particular, virtual screening hits IRE-12 and IRE-13 reduced FLuc bioluminescence intensity to 11% and 32.5%, suggesting their inhibition of IRES-mediated translation were false positives (Figure S6). Thus, we screened the analogs of IRE-03 with ChemFluc server[56] to filter potential FLuc inhibitors. A predicted probability of 0.3 or higher indicates a likelihood of being a strong FLuc inhibitor; thus, all analogs with predicted probabilities above this threshold were excluded. The five shortlisted IRE-03 analogs were tested against FLuc to identify any compounds that may interfere with the assay (Figure S8). While IRE-03-2 and IRE-03-4 expressed inhibition (70% and 30%, respectively) against FLuc, none of the analogs exhibited stronger inhibition than IRE-12. Besides the compounds that inhibited the catalytic activity of FLuc, we also removed IRE-03-4 as it inhibited cap-independent and cap-dependent translation simultaneously (Figures S7, S8). The combination of *in silico* prediction and experimental assay confirmed that both IRE-03-1 and IRE-03-3 are selective inhibitors of EV-A71 IRES and did not interfere with the assay.

In conclusion, our virtual screening against the SL II in EV-A71 IRES has identified potent IRES inhibitors bearing a 3,4-diaryl pyrazole scaffold.. We have also demonstrated the feasibility of applying pharmacophore- and molecular docking-based virtual screening methods typically used

for protein-ligand, for application against an RNA target i.e. the IRES of EV-A71. More excitingly, our studies demonstrate the potential of such approaches in enabling and facilitating future drug discovery efforts for other structured RNA targets.

METHODS

Evaluation of IRES NMR Conformers by Docking

The PDB structure of EV-A71 IRES SL II (PDB: 6XB7) was retrieved from the Protein Data Bank (www.rcsb.org).[67] For each of the five experimentally validated ligands, 50 respective artificial decoys were generated by DUD-E server. To resemble the experimentally validated non-binders, the decoys have similar physicochemical properties (molecular weight, logP, charge, etc.) but distinct topology with the ligand. The parameter logarithmic area under curve (logAUC) reported in the literature[52,68] was applied to assess the performance of molecular docking methods in benchmarking.

MM-GBSA Rescoring

MM-GBSA rescoring was performed with Prime (Prime, Schrödinger, LLC, New York, NY) using OPLS4 forcefield with the Variable Dielectric Surface Generalized Born (VSGB) continuum solvation model applied.[72] The binding free energies for the RNA-ligand complexes were calculated based on the energy terms in the following equation

$$\Delta G_{Bind} = G_{complex} - (G_{receptor} + G_{ligand})$$

where ΔG_{Bind} represents the total binding free energy upon RNA-ligand binding. The complex has not been minimized to avoid changing the PDB structure.

Alignment of EV-A71 IRES conformers was performed with MatchMaker in UCSF ChimeraX,[73] with the alignment algorithm set as “Needleman-Wunsch” and matrix of atoms set as “Nucleic Acid”.

Virtual Screening

The compound library for virtual screening with ~11,000,000 compounds was gathered from ZINC 20 database by combining all “in-stock” compounds with molecular weight between 250-700 Dalton and logP values between 3.5 to -2.5. All ligands and decoys in the benchmarking dataset and all compounds in the virtual screening library were prepared with LigPrep (LigPrep, Schrödinger, LLC, New York, NY) in Schrodinger Suite. All receptor structures used for this study were prepared with PrepWizard (Protein Preparation Wizard, Schrödinger, LLC, NewYork, NY) under the S-OPLS forcefield. Solvent molecules and ions within 6.0 Å of the ligand were deleted. Phase (Phase, Schrödinger, LLC, New York, NY) was applied to generate a pharmacophore model based on the features of the native ligand DMA-135 of EV-A71 IRES PDB structure (PDB: 6XB7). For RxDock 2013.1-1, the docking was performed with command prompt, with the scoring function SF5 applied for all docking runs. The binding cavity is defined as the area 6.0 Å around the reference ligand, and 50 poses were generated for each ligand.

Analog search

To assess the chemical similarity between compounds, Tanimoto coefficients (Tc) were calculated with Daylight-Type fingerprint using Canvas (Canvas, Schrödinger, LLC, New York, NY). A Tc value of less than 0.5 is commonly accepted as an indication of chemical dissimilarity between two compounds. The webserver ChemFluc was applied for filtering potential inhibitors of FLuc.[56]

Chemicals

Resveratrol was purchased from Tokyo-Chemical Industry and prunin-3''-*p*-coumarate (ST077105) was purchased from TimTec. The hit compounds and analogs were purchased from ChemBridge (IRE-01 to 06, IRE-03-1, IRE-03-2, IRE-03-4, IRE-03-5), SigmaAlrich (IRE-03-3) and Vitas M Chemical (IRE-07 to 13). All test compounds were dissolved in dimethyl sulfoxide (DMSO) to make up to either 10 mM or 100 mM stock solutions and stored at -80 °C. Compounds were subjected to no more than 3 freeze-thaw cycles and cells were exposed to DMSO concentrations no higher than 1%.

Cell line, virus and cell culture

Human rhabdomyosarcoma (RD) cells (CCL-136, ATCC) were grown in Dulbecco's Modified Eagle's Medium High Glucose (DMEM; Sigma-Aldrich) supplemented with 10% heat-inactivated fetal calf serum (FCS; 904 PAA) and 2% w/v sodium hydrogen carbonate. DMEM supplemented with 2% FCS and 2% w/v sodium hydrogen carbonate was separately prepared as maintenance media. The virus used in this study is the human enterovirus-A71 (EV-A71) strain 41 (Accession no. AF316321.2), which was propagated in RD cells in maintenance media. All cell cultures were incubated in humidified incubator with growth settings of 37 °C and 5% CO_2, unless otherwise stated.

Evaluation of cell viability

RD cells were seeded at a density of 2 x 104 cells/well onto clear flat-bottom 96-well plates in DMEM supplemented with 10% FCS and allowed to adhere by incubating overnight at the preset growth settings. To initiate the experiment, media was decanted, followed by the addition of 100

µL of drug diluted to working concentration with maintenance media. 1% DMSO and maintenance media alone were added as vehicular and mock controls respectively. The cells were allowed to incubate for further 12 hours, following which, the media was decanted. The cells were then washed once with maintenance media to remove any residual drug before addition of 100 µL 100X alamarBlue™ Cell Viability Reagent prepared by diluting 10X alamarBlue™ Cell Viability Reagent using maintenance media as per manufacturer's recommendations. Cells were then incubated in the dark until vehicular control turned bright pink. The plates were then analysed using an InfiniteTM 200 PRO series microplate reader (Tecan). Fluorescence intensity was measured from the bottom of the plate at excitation and emission wavelengths of 570 nm and 600 nm respectively, and the gain setting set to optimal. Relative cell viability was calculated by normalising measurements from drug-treated to untreated cells.

EV-A71 IRES bicistronic luciferase reporter assay

A bicistronic luciferase reporter assay was previously constructed and validated by our group using the IRES sequence of the EV-A71 strain mentioned.[53] RD cells were seeded at a density of 2 x 10^4 cells/well onto white flat-bottom 96-well plates in DMEM supplemented with 10% FCS and allowed to adhere by incubating overnight at the preset growth settings. Thereafter, the cells were transfected with the bicistronic luciferase reporter construct using jetPRIME transfection reagent (Polypus transfection, Illkirch-Graffenstaden, France) as per manufacturer's recommendations. In brief, the bicistronic luciferase reporter construct (200 ng), jetPRIME transfection reagent (0.4 µL) and jetPRIME buffer (9.6 µL) were first allowed to complex for 10 minutes. Subsequently, the mixture was then diluted 10-fold with maintenance media to make up the transfection mixture. 100 µL transfection mixture was added to each well and allowed to

incubate for 12 h. Post-incubation, media was decanted and replaced with 100 µL of drug diluted to highest non-toxic concentration using maintenance media and allowed to further incubate for 12 h. 0.1% DMSO and prunin-3’’-*p*-coumarate (ST077105)[53] were used as vehicular and positive controls, respectively. Thereafter, the media was decanted and cells washed once with maintenance media followed by luciferase detection using the Dual-Glo® Luciferase Assay System (Promega) as per manufacturer’s recommendations and analyzed using GloMax®-Multi Detection System (Promega) using the built-in Dual-Glo protocol.

Firefly Luciferase inhibition assay

Firefly luciferase (QuantiLum® Recombinant Luciferase, E1701, Lot no. 0000590410, 14.92 mg/mL) was purchased from Promega, stored as per manufacturer's recommendations and used without further purification. The reaction buffer was prepared by dissolving HEPES (BioBasic Asia) powder in water to 150 mM and pH adjusted to 7.5. Dilution buffer was prepared separately by dissolving appropriate amounts of bovine serum albumin (BSA) powder in the reaction buffer to final concentration of 1 mg/mL BSA. Purchased firefly luciferase stock solution was first diluted to 10 µM with dilution buffer and further diluted with reaction buffer to make up 1 µM working stock. Test compounds were diluted to appropriate concentrations with reaction buffer. 1% DMSO and Resveratrol[74,75] was used as vehicular and positive controls, respectively. The assay was performed in white flat-bottom 96-well plates. Each well contained 10 µL firefly luciferase working stock (final concentration 100 nM), 10 µL ONE-Glo EX (Promega) and 10 µL test compounds of appropriate concentrations topped up to 100 µL with reaction buffer. Briefly, appropriate volumes of reaction buffer, firefly luciferase and test compounds were incubated at room temperature for 10 minutes. ONE-Glo EX was then added and incubated for a further 10 minutes. Firefly luciferase activity was analyzed using GloMax®-Multi Detection System (Promega) using the built-in ONE-Glo protocol.

Post-infection drug treatment assay

RD cells were seeded at a density of 2 x 10^4 cells/well onto clear flat bottom 96-well plates in DMEM with 10% FCS and allowed to adhere overnight by incubating at the preset growth settings. The cells were subsequently infected with the EV-A71 virus at multiplicity of infection (MOI) 1, diluted with maintenance media, before incubating at the growth settings for 1 hour. The plates were then washed twice with phosphate-buffered saline. The cells were then allowed to incubate

for 12 h at the preset growth settings with 100 µL of drugs diluted to appropriate concentrations in maintenance media. Post-incubation, the cells were subjected to 2 freeze-thaw cycles (-80 °C; 37 °C) for cell lysis to obtain viral supernatant for subsequent viral plaque reduction assay.

Viral plaque reduction assay

RD cells were seeded at a density of 2.5 x 10^5 cells/well onto clear 24-well plates in DMEM with 10% FCS and allowed to adhere overnight by incubating at the preset growth settings. Harvested viral supernatant was serially diluted in 10-fold dilutions to obtain final concentrations ranging from 10^{-1} to 10^{-6} in maintenance media. RD cells were then incubated with 100 µL viral supernatant of appropriate dilutions for 1 hour at the growth settings. Then, the plates were washed twice with phosphate-buffered saline before the addition of 0.5 mL overlay medium containing 0.5% agarose in maintenance media. The plates were incubated for 2 days at the growth settings before being subjected to cell fixing and staining with 4% paraformaldehyde/1% crystal violet solution (Sigma-Aldrich) at 25 °C. Plaques were then visualized as clear patches within the stained cells and quantified by counting. The counted plaques were multiplied by the respective dilution factors to determine the viral titer, presented as plaque forming units per milliliter (PFU/mL).

Nanoluciferase replicon reporter assay

Purified EV-A71 replication-competent and replication-defective RNA replicons were produced as per a previously established protocol in our group.[57] RD cells were seeded at a density of 2 x 10^4 cells/well onto white flat-bottom 96-well plates in DMEM supplemented with 10% FCS and allowed to adhere by incubating overnight at the preset growth settings. Thereafter, the cells were transfected with the respective EV-A71 replicons using DharmaFECT-1 transfection reagent (Thermo Scientific). In brief, the respective EV-A71 replicon (200 ng), DharmaFECT-1 transfection reagent (0.5 µL) and serum-free DMEM (49.5 µL) were first allowed to complex for

20 minutes. Following which, growth media was decanted from the wells and topped up with 100 µL maintenance media. 50 µL of transfection mixture were then added to each well and allowed to incubate for 6 h. Post-incubation, media was decanted and replaced with 100 µL of drug diluted to appropriate concentrations using maintenance media and allowed to further incubate for 12 h. 0.1% DMSO was used as vehicular controls while guanidine hydrochloride (GuHCl) and cycloheximide (CHX) were used as positive controls for RNA replication and general translation, respectively. Thereafter, the media was decanted and cells washed once with maintenance media followed by luciferase detection using the Nano-Glo® Luciferase Assay System (Promega) as per manufacturer's recommendations and analyzed using GloMax®-Multi Detection System (Promega) using the built-in Nano-Glo protocol.

SUPPORTING INFORMATION

- Superposition of ligand-complexed NMR conformers of EV-A71 IRES SL II (PDB: 6XB7); Pharmacophore modelling of EV-A71 IRES SL II native ligand and selection of initial virtual screening hits (IRE-01 to IRE-13); Cytotoxicity profiles, FLuc enzyme inhibition assay, RLuc bioluminescence values from the bicistronic reporter assay and nanoluciferase replicon reporter assay results of selected compounds.

- SMILES molecular formula strings of all compounds tested.

AUTHOR CONTRIBUTIONS

Wang Kaichen – Conceptualization, Computational studies, Writing and editing of manuscript;

Sean Xian Yu Lee – Biological studies, Writing and editing of manuscript;

Chaitanya K. Jaladanki – Computational studies;

Wei Shen Ho – Biological studies;

Justin Jang Hann Chu – Supervision, Advice on biological studies;

Hao Fan – Conceptualization, Supervision, Writing and editing of manuscript;

Christina Li Lin Chai – Conceptualizataion, Supervision, Writing and editing of manuscript

CONFLICT OF INTEREST

The authors declare no conflicts of interest.

ACKNOWLEDGEMENTS

This project was supported by the Ministry of Education, Singapore, under the Academic Research Fund Tier 1 (FY 2024) and MOE-T2EP30221-0005. Grant number: A-8001493-00-00 to CLLC. H.F. and C.K.J. were also supported by Biomedical Research Council of Agency for

Science, Technology and Research (A*STAR), Singapore. The authors would also like to thank Dr. Thinessh Yogarajah and Ms. Jasmaadiyah Binte Habib Mohameed (Laboratory of Molecular RNA Virology and Antiviral Strategies, National University of Singapore, Singapore) for their kind provision of the EV-A71 replicons and IRES plasmids for biological studies.

ASSOCIATED CONTENTS

Data and Software Availability Statement

The protein structure (PDB ID: 6XB7 − 10.2210/pdb6XB7/pdb) used for virtual screening was obtained from the RCSB protein databank.[71] UCSF ChimeraX (https://www.cgl.ucsf.edu/chimerax/) was applied for superimposing the NMR conformers and RMSD calculation.[73] Molecular docking was performed with RxDock 2013.1-1.[51] MM-GBSA rescoring, pharmacophore screening, clustering of compounds and visualization of docking poses was performed in Schrödinger 2024.2 (https://www.schrodinger.com/) suite. ChemFluc (http://admet.scbdd.com/chemfluc/index/) webserver was applied to filter compounds that could inhibit the enzymatic activity of FLuc.[56] Additional information will be made available upon request to the corresponding authors.

REFERENCES

(1) Pavlova, N.; Kaloudas, D.; Penchovsky, R. Riboswitch Distribution, Structure, and Function in Bacteria. *Gene* **2019**, *708*, 38–48.

(2) Peselis, A.; Serganov, A. Themes and Variations in Riboswitch Structure and Function. *Biochim. Biophys. Acta, Gene Regul. Mech.* **2014**, *1839* (10), 908–918.

(3) Kavita, K.; Breaker, R. R. Discovering Riboswitches: The Past and the Future. *Trends Biochem. Sci.* **2023**, *48* (2), 119–141.

(4) Davis, B.; Afshar, M.; Varani, G.; Murchie, A. I. H.; Karn, J.; Lentzen, G.; Drysdale, M.; Bower, J.; Potter, A. J.; Starkey, I. D.; Swarbrick, T.; Aboul-ela, F., Rational Design of Inhibitors of HIV-1 TAR RNA through the Stabilisation of Electrostatic "Hot Spots". *J. Mol. Biol.* **2004,** *336* (2), 343-356.

(5) Sosic, A.; Frecentese, F.; Perissutti, E.; Sinigaglia, L.; Santagada, V.; Caliendo, G.; Magli, E.; Ciano, A.; Zagotto, G.; Parolin, C.; Gatto, B., Design, synthesis and biological evaluation of TAR and cTAR binders as HIV-1 nucleocapsid inhibitors. *MedChemComm* **2013,** *4* (10), 1388-1393.

(6) Abulwerdi, F. A.; Shortridge, M. D.; Sztuba-Solinska, J.; Wilson, R.; Le Grice, S. F. J.; Varani, G.; Schneekloth, J. S., Jr., Development of Small Molecules with a Noncanonical Binding Mode to HIV-1 Trans Activation Response (TAR) RNA. *J. Med. Chem.* **2016,** *59* (24), 11148-11160.

(7) Zeiger, M.; Stark, S.; Kalden, E.; Ackermann, B.; Ferner, J.; Scheffer, U.; Shoja-Bazargani, F.; Erdel, V.; Schwalbe, H.; Göbel, M. W., Fragment based search for small molecule inhibitors of HIV-1 Tat-TAR. *Bioorg. Med. Chem. Lett.* **2014,** *24* (24), 5576-5580.

(8) Alanazi, A.; Ivanov, A.; Kumari, N.; Lin, X.; Wang, S.; Kovalskyy, D.; Nekhai, S., Targeting Tat–TAR RNA Interaction for HIV-1 Inhibition. *Viruses* **2021,** *13* (10), 2004.

(9) Abulwerdi, F. A.; Xu, W.; Ageeli, A. A.; Yonkunas, M. J.; Arun, G.; Nam, H.; Schneekloth, J. S., Jr.; Dayie, T. K.; Spector, D.; Baird, N.; Le Grice, S. F. J., Selective Small-Molecule Targeting of a Triple Helix Encoded by the Long Noncoding RNA, MALAT1. *ACS Chem. Biol.* **2019,** *14* (2), 223-235.

(10) Amodio, N.; Raimondi, L.; Juli, G.; Stamato, M. A.; Caracciolo, D.; Tagliaferri, P.; Tassone, P., MALAT1: a druggable long non-coding RNA for targeted anti-cancer approaches. *J. Hematol. Oncol.* **2018,** *11* (1), 63.

(11) Zhang, X.; Hamblin, M. H.; Yin, K. J., The long noncoding RNA Malat1: Its physiological and pathophysiological functions. *RNA Biol.* **2017,** *14* (12), 1705-1714.

(12) Rigo, F.; Hua, Y.; Krainer, A. R.; Bennett, C. F., Antisense-based therapy for the treatment of spinal muscular atrophy. *J. Cell. Biol.* **2012,** *199* (1), 21-5.

(13) Crooke, S. T.; Baker, B. F.; Crooke, R. M.; Liang, X.-H., Antisense technology: an overview and prospectus. *Nat. Rev. Drug Discovery* **2021,** *20* (6), 427-453.

(14) Zhang, J.; Chen, B.; Gan, C.; Sun, H.; Zhang, J.; Feng, L., A Comprehensive Review of Small Interfering RNAs (siRNAs): Mechanism, Therapeutic Targets, and Delivery Strategies for Cancer Therapy. *Int. J. Nanomed.* **2023,** *18*, 7605-7635.

(15) Agrawal, N.; Dasaradhi, P. V. N.; Mohmmed, A.; Malhotra, P.; Bhatnagar Raj, K.; Mukherjee Sunil, K., RNA Interference: Biology, Mechanism, and Applications. *Microbiol. Mol. Biol. Rev.* **2003,** *67* (4), 657-685.

(16) Childs-Disney, J. L.; Yang, X.; Gibaut, Q. M. R.; Tong, Y.; Batey, R. T.; Disney, M. D., Targeting RNA structures with small molecules. *Nat. Rev. Drug Discovery* **2022,** *21* (10), 736-762.

(17) Rizvi, N. F.; Santa Maria, J. P.; Nahvi, A.; Klappenbach, J.; Klein, D. J.; Curran, P. J.; Richards, M. P.; Chamberlin, C.; Saradjian, P.; Burchard, J.; Aguilar, R.; Lee, J. T.; Dandliker, P. J.; Smith, G. F.; Kutchukian, P.; Nickbarg, E. B., Targeting RNA with Small Molecules:

Identification of Selective, RNA-Binding Small Molecules Occupying Drug-Like Chemical Space. *SLAS Discovery* **2019,** *25* (4), 384-396.

(18) Sheridan, C., First small-molecule drug targeting RNA gains momentum. *Nat. Biotechnol.* **2021,** *39* (1), 6-8.

(19) Auerbach-Nevo, T.; Baram, D.; Bashan, A.; Belousoff, M.; Breiner, E.; Davidovich, C.; Cimicata, G.; Eyal, Z.; Halfon, Y.; Krupkin, M.; Matzov, D.; Metz, M.; Rufayda, M.; Peretz, M.; Pick, O.; Pyetan, E.; Rozenberg, H.; Shalev-Benami, M.; Wekselman, I.; Zarivach, R.; Zimmerman, E.; Assis, N.; Bloch, J.; Israeli, H.; Kalaora, R.; Lim, L.; Sade-Falk, O.; Shapira, T.; Taha-Salaime, L.; Tang, H.; Yonath, A., Ribosomal Antibiotics: Contemporary Challenges. *Antibiotics (Basel, Switz.)* **2016,** *5* (3), 24.

(20) Wang, H.; Mann, P. A.; Xiao, L.; Gill, C.; Galgoci, A. M.; Howe, J. A.; Villafania, A.; Barbieri, C. M.; Malinverni, J. C.; Sher, X.; Mayhood, T.; McCurry, M. D.; Murgolo, N.; Flattery, A.; Mack, M.; Roemer, T., Dual-Targeting Small-Molecule Inhibitors of the *Staphylococcus aureus* FMN Riboswitch Disrupt Riboflavin Homeostasis in an Infectious Setting. *Cell Chem. Biol.* **2017,** *24* (5), 576-588.e6.

(21) Motika, S. E.; Ulrich, R. J.; Geddes, E. J.; Lee, H. Y.; Lau, G. W.; Hergenrother, P. J., Gram-Negative Antibiotic Active Through Inhibition of an Essential Riboswitch. *J. Am. Chem. Soc.* **2020,** *142* (24), 10856-10862.

(22) Connelly, C. M.; Numata, T.; Boer, R. E.; Moon, M. H.; Sinniah, R. S.; Barchi, J. J.; Ferré-D'Amaré, A. R.; Schneekloth, J. S., Synthetic ligands for PreQ1 riboswitches provide structural and mechanistic insights into targeting RNA tertiary structure. *Nat. Commun.* **2019,** *10* (1), 1501.

(23) Xu, L.; Xiao, Y.; Zhang, J.; Fang, X., Structural insights into translation regulation by the THF-II riboswitch. *Nucleic Acids Res.* **2023,** *51* (2), 952-965.

(24) Trausch, J. J.; Batey, R. T., A disconnect between high-affinity binding and efficient regulation by antifolates and purines in the tetrahydrofolate riboswitch. *Chem. Biol.* **2014,** *21* (2), 205-16.

(25) Dibrov, S. M.; Parsons, J.; Carnevali, M.; Zhou, S.; Rynearson, K. D.; Ding, K.; Garcia Sega, E.; Brunn, N. D.; Boerneke, M. A.; Castaldi, M. P.; Hermann, T., Hepatitis C virus translation inhibitors targeting the internal ribosomal entry site. *J. Med. Chem.* **2014,** *57* (5), 1694-707.

(26) Parsons, J.; Castaldi, M. P.; Dutta, S.; Dibrov, S. M.; Wyles, D. L.; Hermann, T., Conformational inhibition of the hepatitis C virus internal ribosome entry site RNA. *Nat. Chem. Biol.* **2009,** *5* (11), 823-825.

(27) Neupane, K.; Munshi, S.; Zhao, M.; Ritchie, D. B.; Ileperuma, S. M.; Woodside, M. T., Anti-Frameshifting Ligand Active against SARS Coronavirus-2 Is Resistant to Natural Mutations of the Frameshift-Stimulatory Pseudoknot. *J. Mol. Biol.* **2020,** *432* (21), 5843-5847.

(28) Mercuri, E.; Pera, M. C.; Scoto, M.; Finkel, R.; Muntoni, F., Spinal muscular atrophy — insights and challenges in the treatment era. *Nat. Rev. Neurol.* **2020,** *16* (12), 706-715.

(29) Ratni, H.; Ebeling, M.; Baird, J.; Bendels, S.; Bylund, J.; Chen, K. S.; Denk, N.; Feng, Z.; Green, L.; Guerard, M.; Jablonski, P.; Jacobsen, B.; Khwaja, O.; Kletzl, H.; Ko, C.-P.; Kustermann, S.; Marquet, A.; Metzger, F.; Mueller, B.; Naryshkin, N. A.; Paushkin, S. V.; Pinard, E.; Poirier, A.; Reutlinger, M.; Weetall, M.; Zeller, A.; Zhao, X.; Mueller, L., Discovery of

Risdiplam, a Selective Survival of Motor Neuron-2 (SMN2) Gene Splicing Modifier for the Treatment of Spinal Muscular Atrophy (SMA). *J. Med. Chem.* **2018,** *61* (15), 6501-6517.

(30) Ratni, H.; Scalco, R. S.; Stephan, A. H., Risdiplam, the First Approved Small Molecule Splicing Modifier Drug as a Blueprint for Future Transformative Medicines. *ACS Med. Chem. Lett.* **2021,** *12* (6), 874-877.

(31) Klebe, G., Virtual ligand screening: strategies, perspectives and limitations. *Drug Discovery Today* **2006,** *11* (13), 580-594.

(32) Bajorath, J., Integration of virtual and high-throughput screening. *Nat. Rev. Drug Discovery* **2002,** *1* (11), 882-894.

(33) Park, H.-J.; Park, S.-J., Virtual Screening for RNA-Interacting Small Molecules. In *Biophysical approaches to translational control of gene expression*, Dinman, J. D., Ed. Springer New York: New York, NY, 2013; pp 235-252.

(34) Kallert, E.; Fischer, T. R.; Schneider, S.; Grimm, M.; Helm, M.; Kersten, C., Protein-Based Virtual Screening Tools Applied for RNA–Ligand Docking Identify New Binders of the preQ1-Riboswitch. *J. Chem. Inf. Model.* **2022,** *62* (17), 4134-4148.

(35) Park, S.-J.; Kim, Y.-G.; Park, H.-J., Identification of RNA Pseudoknot-Binding Ligand That Inhibits the −1 Ribosomal Frameshifting of SARS-Coronavirus by Structure-Based Virtual Screening. *J. Am. Chem. Soc.* **2011,** *133* (26), 10094-10100.

(36) Luo, J.; Wei, W.; Waldispühl, J.; Moitessier, N., Challenges and current status of computational methods for docking small molecules to nucleic acids. *Eur. J. Med. Chem.* **2019,** *168*, 414-425.

(37) Tessaro, F.; Scapozza, L., How 'Protein-Docking' Translates into the New Emerging Field of Docking Small Molecules to Nucleic Acids? *Molecules* **2020,** *25* (12), 2749.

(38) Cao, Z.; Zeng, D.; Wang, Q.; Zheng, X.; Wang, F., An epidemiological analysis of the Beijing 2008 Hand-Foot-Mouth epidemic. *Chin. Sci. Bull.* **2010,** *55* (12), 1142-1149.

(39) Liu, M.; Xu, B.; Ma, Y.; Shang, L.; Ye, S.; Wang, Y., Reversible covalent inhibitors suppress enterovirus 71 infection by targeting the 3C protease. *Antiviral Res.* **2021,** *192,* 105102.

(40) Wang, Y.; Cao, L.; Zhai, Y.; Ma, J.; Nie, Q.; Li, T.; Yin, Z.; Sun, Y.; Shang, L., Inhibition of enterovirus 71 replication by an α-hydroxy-nitrile derivative NK-1.9k. *Antiviral Res.* **2017,** *141*, 91-100.

(41) Ho, J.-Y.; Chern, J.-H.; Hsieh, C.-F.; Liu, S.-T.; Liu, C.-J.; Wang, Y.-S.; Kuo, T.-W.; Hsu, S.-J.; Yeh, T.-K.; Shih, S.-R.; Hsieh, P.-W.; Chiu, C.-H.; Horng, J.-T., In vitro and in vivo studies of a potent capsid-binding inhibitor of enterovirus 71. *J. Antimicrob. Chemother.* **2016,** *71* (7), 1922-1932.

(42) Shia, K.-S.; Li, W.-T.; Chang, C.-M.; Hsu, M.-C.; Chern, J.-H.; Leong, M. K.; Tseng, S.-N.; Lee, C.-C.; Lee, Y.-C.; Chen, S.-J.; Peng, K.-C.; Tseng, H.-Y.; Chang, Y.-L.; Tai, C.-L.; Shih, S.-R., Design, Synthesis, and Structure−Activity Relationship of Pyridyl Imidazolidinones: A Novel Class of Potent and Selective Human Enterovirus 71 Inhibitors. *J. Med. Chem.* **2002,** *45* (8), 1644-1655.

(43) Li, P.; Yu, J.; Hao, F.; He, H.; Shi, X.; Hu, J.; Wang, L.; Du, C.; Zhang, X.; Sun, Y.; Lin, F.; Gu, Z.; Xu, D.; Chen, X.; Shen, L.; Hu, G.; Li, J.; Chen, S.; Xiao, W.; Wang, Z.; Guo, Q.; Chang,

X.; Tian, X.; Lin, T., Discovery of Potent EV71 Capsid Inhibitors for Treatment of HFMD. *ACS Med. Chem. Lett.* **2017,** *8* (8), 841-846.

(44) Deng, C.-L.; Yeo, H.; Ye, H.-Q.; Liu, S.-Q.; Shang, B.-D.; Gong, P.; Alonso, S.; Shi, P.-Y.; Zhang, B., Inhibition of enterovirus 71 by adenosine analog NITD008. *J. Virol.* **2014,** *88* (20), 11915-11923.

(45) Lee, K.-M.; Chen, C.-J.; Shih, S.-R. Regulation Mechanisms of Viral IRES-Driven Translation. *Trends Microbiol.* **2017**, *25* (7), 546–561.

(46) Martinez-Salas, E.; Francisco-Velilla, R.; Fernandez-Chamorro, J.; Embarek, A. M., Insights into Structural and Mechanistic Features of Viral IRES Elements. *Front. Microbiol.* **2018,** *8*.

(47) Tolbert, M.; Morgan, C. E.; Pollum, M.; Crespo-Hernández, C. E.; Li, M.-L.; Brewer, G.; Tolbert, B. S., HnRNP A1 Alters the Structure of a Conserved Enterovirus IRES Domain to Stimulate Viral Translation. *J. Mol. Biol.* **2017,** *429* (19), 2841-2858.

(48) Levengood, J. D.; Tolbert, M.; Li, M.-L.; Tolbert, B. S., High-affinity interaction of hnRNP A1 with conserved RNA structural elements is required for translation and replication of enterovirus 71. *RNA Biol.* **2013,** *10* (7), 1136-1145.

(49) Davila-Calderon, J.; Patwardhan, N. N.; Chiu, L.-Y.; Sugarman, A.; Cai, Z.; Penutmutchu, S. R.; Li, M.-L.; Brewer, G.; Hargrove, A. E.; Tolbert, B. S., IRES-targeting small molecule inhibits enterovirus 71 replication via allosteric stabilization of a ternary complex. *Nat. Commun.* **2020,** *11* (1), 4775.

(50) Irwin, J. J.; Tang, K. G.; Young, J.; Dandarchuluun, C.; Wong, B. R.; Khurelbaatar, M.; Moroz, Y. S.; Mayfield, J.; Sayle, R. A., ZINC20—A Free Ultralarge-Scale Chemical Database for Ligand Discovery. *J. Chem. Inf. Model.* **2020,** *60* (12), 6065-6073.

(51) Ruiz-Carmona, S.; Alvarez-Garcia, D.; Foloppe, N.; Garmendia-Doval, A. B.; Juhos, S.; Schmidtke, P.; Barril, X.; Hubbard, R. E.; Morley, S. D., rDock: A Fast, Versatile and Open Source Program for Docking Ligands to Proteins and Nucleic Acids. *PLoS Comput. Biol.* **2014,** *10* (4), e1003571.

(52) Mysinger, M. M.; Carchia, M.; Irwin, J. J.; Shoichet, B. K., Directory of Useful Decoys, Enhanced (DUD-E): Better Ligands and Decoys for Better Benchmarking. *J. Med. Chem.* **2012,** *55* (14), 6582-6594.

(53) Gunaseelan, S.; Wong, K. Z.; Min, N.; Sun, J.; Ismail, N. K. B. M.; Tan, Y. J.; Lee, R. C. H.; Chu, J. J. H., Prunin suppresses viral IRES activity and is a potential candidate for treating enterovirus A71 infection. *Sci. Transl. Med.* **2019,** *11* (516), eaar5759.

(54) Francisco-Velilla, R.; Embarc-Buh, A.; Abellan, S.; Martinez-Salas, E. Picornavirus Translation Strategies. *FEBS Open Bio.* **2022**, *12* (6), 1125–1141.

(55) Auld, D. S.; Inglese, J., Interferences with Luciferase Reporter Enzymes. In *Assay Guidance Manual*, Markossian, S.; Grossman, A.; Arkin, M.; Auld, D.; Austin, C.; Baell, J.; Brimacombe, K.; Chung, T. D. Y.; Coussens, N. P.; Dahlin, J. L.; Devanarayan, V.; Foley, T. L.; Glicksman, M.; Gorshkov, K.; Haas, J. V.; Hall, M. D.; Hoare, S.; Inglese, J.; Iversen, P. W.; Lal-Nag, M.; Li, Z.; Manro, J. R.; McGee, J.; McManus, O.; Pearson, M.; Riss, T.; Saradjian, P.; Sittampalam, G. S.; Tarselli, M.; Trask, O. J., Jr.; Weidner, J. R.; Wildey, M. J.; Wilson, K.; Xia, M.; Xu, X., Eds.

Eli Lilly & Company and the National Center for Advancing Translational Sciences: Bethesda (MD), 2004.

(56) Yang, Z.-Y.; Dong, J.; Yang, Z.-J.; Lu, A.-P.; Hou, T.-J.; Cao, D.-S. Structural Analysis and Identification of False Positive Hits in Luciferase-Based Assays. *J. Chem. Inf. Model.* **2020**, *60* (4), 2031–2043.

(57) Wu, K. X.; Chu, J. J.-H. Antiviral screen identifies EV71 inhibitors and reveals camptothecin-target, DNA topoisomerase 1 as a novel EV71 host factor. *Antiviral Res*. **2017**, 143, 122-133.

(58) Lim, T. Y. M.; Jaladanki, C. K.; Wong, Y. H.; Yogarajah, T.; Fan, H.; Chu, J. J. H. Tanomastat Exerts Multi-Targeted Inhibitory Effects on Viral Capsid Dissociation and RNA Replication in Human Enteroviruses. *eBioMedicine* **2024**, 107, 105277.

(59) Murray, K. E.; Nibert, M. L. Guanidine Hydrochloride Inhibits Mammalian Orthoreovirus Growth by Reversibly Blocking the Synthesis of Double-Stranded RNA. *J Virol.* **2007**, *81* (9), 4572–4584.

(60) Schneider-Poetsch, T.; Ju, J.; Eyler, D. E.; Dang, Y.; Bhat, S.; Merrick, W. C.; Green, R.; Shen, B.; Liu, J. O. Inhibition of Eukaryotic Translation Elongation by Cycloheximide and Lactimidomycin. *Nat. Chem. Biol.* **2010**, *6* (3), 209–217.

(61) Li, G.; De Clercq, E., Overview of Antiviral Drug Discovery and Development: Viral Versus Host Targets. In *Antiviral Discovery for Highly Pathogenic Emerging Viruses*, Muñoz-Fontela, C.; Delgado, R., Eds. The Royal Society of Chemistry: 2021; p 0.

(62) Hermann, T., Small molecules targeting viral RNA. *WIREs RNA* **2016,** *7* (6), 726-743.

(63) Fan, H.; Irwin, J. J.; Webb, B. M.; Klebe, G.; Shoichet, B. K.; Sali, A. Molecular Docking Screens Using Comparative Models of Proteins. *J. Chem. Inf. Model.* **2009**, *49* (11), 2512–2527.

(64) Rettenmaier, T. J.; Fan, H.; Karpiak, J.; Doak, A.; Sali, A.; Shoichet, B. K.; Wells, J. A. Small-Molecule Allosteric Modulators of the Protein Kinase PDK1 from Structure-Based Docking. *J. Med. Chem.* **2015**, *58* (20), 8285–8291.

(65) Amaro, R. E.; Baudry, J.; Chodera, J.; Demir, Ö.; McCammon, J. A.; Miao, Y.; Smith, J. C., Ensemble Docking in Drug Discovery. *Biophys. J.* **2018,** *114* (10), 2271-2278.

(66) Kallert, E.; Almena Rodriguez, L.; Husmann, J.-Å.; Blatt, K.; Kersten, C., Structure-based virtual screening of unbiased and RNA-focused libraries to identify new ligands for the HCV IRES model system. *RSC Med. Chem.* **2024,** *15* (5), 1527-1538.

(67) Renner, S.; Ludwig, V.; Boden, O.; Scheffer, U.; Göbel, M.; Schneider, G., New Inhibitors of the Tat–TAR RNA Interaction Found with a “Fuzzy” Pharmacophore Model. *ChemBioChem* **2005,** *6* (6), 1119-1125.

(68) Thorne, N.; Inglese, J.; Auld, D. S. Illuminating Insights into Firefly Luciferase and Other Bioluminescent Reporters Used in Chemical Biology. *Chem. & Biol.* **2010**, *17* (6), 646–657.

(69) Auld, D. S.; Thorne, N.; Nguyen, D. T.; Inglese, J., A specific mechanism for nonspecific activation in reporter-gene assays. *ACS Chem. Biol.* **2008,** *3* (8), 463-70.

(70) Wu, G.-Q.; Wang, X.; Zhou, H.-Y.; Chai, K.-Q.; Xue, Q.; Zheng, A.-H.; Zhu, X.-M.; Xiao, J.-Y.; Ying, X.-H.; Wang, F.-W.; Rui, T.; Xu, L.-Y.; Zhang, Y.-K.; Liao, Y.-J.; Xie, D.; Lu, L.-Q.; Huang, D.-S., Evidence for transcriptional interference in a dual-luciferase reporter system. *Sci. Rep.* **2015,** *5* (1), 17675.

(71) Berman, H. M.; Westbrook, J.; Feng, Z.; Gilliland, G.; Bhat, T. N.; Weissig, H.; Shindyalov, I. N.; Bourne, P. E., The Protein Data Bank. *Nucleic Acids Res.* **2000,** *28* (1), 235-242.

(72) Li, J.; Abel, R.; Zhu, K.; Cao, Y.; Zhao, S.; Friesner, R. A., The VSGB 2.0 Model: A next Generation Energy Model for High Resolution Protein Structure Modeling. *Proteins: Struct., Funct., Genet*. **2011**, 79 (10), 2794– 2812

(73) Meng, E. C.; Goddard, T. D.; Pettersen, E. F.; Couch, G. S.; Pearson, Z. J.; Morris, J. H.; Ferrin, T. E., UCSF ChimeraX: Tools for structure building and analysis. *Prot. Sci.* **2023,** *32* (11), e4792.

(74) Bakhtiarova, A.; Taslimi, P.; Elliman, S. J.; Kosinski, P. A.; Hubbard, B.; Kavana, M.; Kemp, D. M., Resveratrol inhibits firefly luciferase. *Biochem. Biophys. Res. Commun.* **2006,** *351* (2), 481-484.

(75) Bedford, R.; LePage, D.; Hoffmann, R.; Kennedy, S.; Gutschenritter, T.; Bull, L.; Sujijantarat, N.; DiCesare, J. C.; Sheaff, R. J., Luciferase inhibition by a novel naphthoquinone. *J. Photochem. Photobiol., B* **2012,** *107*, 55-64.